Comparing and Benchmarking Fatigue Behaviours of Various SAC Solders under Thermo-Mechanical Loading

Joshua Adeniyi Depiver
School of Mechanical Engineering & the Built Environment
College of Engineering & Technology
University of Derby, Derby, United Kingdom
J.Depiver@derby.ac.uk

Sabuj Mallik
School of Mechanical Engineering & the Built Environment
College of Engineering & Technology
University of Derby, Derby, United Kingdom
S.Mallik@derby.ac.uk

Emeka H. Amalu
Department of Engineering, School of Computing, Engineering and Digital Technologies, Teesside University
Middlesbrough, Tees Valley, United Kingdom
E.Amalu@tees.ac.uk

***Abstract*— While the fatigue behaviours (including fatigue life predictions) of lead-free solder joints have been extensively researched in the last 15 years, these are not adequately compared and benchmarked for different lead-free solders that are being used. As more and more fatigue properties of lead-free solders are becoming available, it is also critical to know how fatigue behaviours differ under different mathematical models. This paper addresses the challenges and presents a comparative study of fatigue behaviours of various mainstream lead-free Sn-Ag-Cu (SAC) solders and benchmarked those with lead-based eutectic solder. Creep-induced fatigue and fatigue life of lead-based eutectic Sn63Pb37 and four lead-free SAC solder alloys: SAC305, SAC387, SAC396 and SAC405 are analysed through simulation studies. The Anand model is used to simulate the inelastic deformation behaviour of the solder joints under accelerated thermal cycling (ATC). It unifies the creep and rate-independent plastic behaviour and it is used to predict the complex stress-strain relationship of solders under different temperatures and strain rates, which are required in the prediction of fatigue life using the fatigue life models such as Engelmaier, Coffin-Mason and Solomon as the basis of our comparison. The ATC was carried out using temperature range from $-40℃$ to $150℃$. The fatigue damage propagation is determined with finite element (FE) simulation, which allows virtual prototyping in the design process of electronics devices. The simulation was carried out on a BGA (36 balls, 6×6 matrix) mounted onto Cu padded substrate. Results are analysed for plastic strain, Von mises stress, strain energy density, and stress-strain hysteresis loop. The simulation results show that the fatigue behaviours of lead-based eutectic Sn63Pb37 solder is comparable to those of lead-free SAC solders. Among the four SAC solders, SAC387 consistently produced higher plastic strain, strain energy and stress than the other solders. The fatigue life's estimation of the solder joint was investigated using Engelmaier, Coffin-Manson, and Solomon models. Results obtained show that SAC405 has the highest fatigue life (25.7, 21.1 and 19.2 years) followed by SAC396 (18.7, 20.3 and 17.9 years) and SAC305 (15.2, 13.6 and 16.2 years) solder alloys respectively. Predicting the fatigue life of these solder joints averts problems in electronics design for reliability and quality, which if not taken care of, may result in lost revenue. Predictive fatigue analysis can also considerably reduce premature failure, and modern analysis technique such as one used in this research is progressively helping to provide comprehensive product life expectancy data.**

Keywords— Fatigue, Von mises stress, Strain energy density, Hysteresis loop, Plastic strain

I. INTRODUCTION

The long-term reliability of electronic devices is often limited by the fatigue failure of solder interconnects due to thermal cycling or isothermal ageing. In electronic assemblies, solder joints are subjected to thermal, electrical and mechanical cycling, which lead to the fatigue failure of solder joints involving crack initiation, crack propagation, damage accumulation, and failure. Solder fatigue is defined as the mechanical degradation of solder due to deformation under cyclic loading. Thermal cycling and isothermal ageing lead to significant changes in the mechanical behaviour of solder joints utilised in safety-critical applications such as aeroplane, defence, oil & gas drilling applications, underhood of an automobile, medical devices, power grids and so forth. The most common approach to the assessment of fatigue life is based on conducting an accelerated thermal test. Because solder joints are applied at high temperatures and miniature, their reliability is of significant interest to electronics manufacturing engineers and industries. When solder joints remain in conformance with their mechanical, electrical and visual specifications over a specified duration, under a specific set of operational provisions, that is to referred solder joint reliability. Reliability of these solder joints is defined by multiple factors such as shear strength, creep resistance, drop shock, thermal fatigue and vibration resistance. Due to the adoption of the Restriction of Hazardous Substances (RoHS) (also known as Directive 2002/95/EC) directives on 1 July 2006, by the European Union (EU), there have been significant progress in the developments of lead-free solders as a replacement for the conventional lead-based solders for application in the electronics industries [1]–[5] because lead (Pb) was discovered to be one of the leading 17 chemicals that posed an enormous hazard to human life and environment by the EU. Amongst the lead-free solders investigated, Sn-Ag and Sn-Ag-Cu (SAC) based solders offer the most promising characteristics as replacement of lead-based eutectic solder [6], [7].

Solder interconnections are typically exposed to different real-life state such as vibration, drop, thermal shock, elevated temperature, and changing temperature conditions. All the conditions stated have been established as threats for solder joints reliability and the thermal cycling has been identified as the main threat [8]–[12]. When solder joints are at extremely high temperature, creep failure dominates; and when they are exposed to thermal cycling, fatigue failure dominates [13]–[20]. If under the combination of both the failure mechanism is usually referred to as creep-fatigue [21]. The creep and fatigue of solder joints are essentially due to the mismatch of coefficient of thermal extension (CTE) between the BGA component and PCB. The degradation of

solder joints due to different CTE of joined materials has been a known issue in the electronics industry since the basic design of modern electronic in the late 1950s/early 1960s [22]. When a system undergoes thermal cycling, fatigue is said to occur when a system fails or malfunction. FEM has become the common tool used in the analyses of solder joint fatigue failure and reliability in the electronics industries [23]–[26]. During exposure to thermal cycling, fatigue is mainly due to the thermomechanical stresses in the solder joints arising from the differences in the CTE between PCB and components [27], [28].

Awareness and knowledge of the failure mechanisms of these systems are necessary for preventing accidents [29] and the cyclical variation of thermal stress effects solders joint thermal fatigue failure. Throughout thermal cycling, creep is the primary tool of thermal deformation fatigue failure. With ambient temperature changes (e.g. temperature periodicity rises and fall) or part emits heat (e.g. systematic power on and off), solder joints will produce thermal stress. In the development of thermal cycling, creep is the critical process of thermal deformation fatigue failure [30]. Different researchers have studied the effect of ageing on the fatigue, and mechanical properties of solder interconnect. The vital influence of ageing was found on shear strength, drop fatigue performance, thermal cycling reliability, fracture behaviour, microstructure, hardness, creep behaviour, and cyclic shear reliability [19], [31]–[43].

In this study, the Anand viscoplastic constitutive model has been used in the prediction of five solder alloys (lead-based eutectic Sn63Pb37 and lead-free SAC (SAC305, SAC387, SAC396 and SAC405) solders using FEA simulation to determine the damage parameter (plastic strain range). The Engelmaier modified fatigue model, an improved version of Coffin-Manson model takes the thermal cycle frequency, temperature effect and elastic-plastic strain into account and was used to determine the fatigue life of the solders considered in this investigation. The Solomon model however only consider damage parameter of shear strain applicable to 60/40 eutectic solder or near eutectic solder alloy materials with low cycle fatigue applicable condition thus would not be appropriate to use it for the evaluation of fatigue life for the solder alloy materials considered in this research. Analytical models in engineering have several practical uses: 1) rapid design optimization during the development phase of a product, 2) predicting field use limits, and 3) failure analysis of product returned from the field or failed in a qualification test [44], [45].

II. FATIGUE LIFE PREDICTION MODELS

The fatigue life of solder joint alloy materials subjected to thermal cycling is ordinarily predicted employing fatigue life prediction models such as the hyperbolic sine constitutive equation as the constitutive equation is a damage mechanism-based life prediction model. The principal damage mechanism for SAC solder throughout the thermal cycling operation is a creep; also, it is applied to simulate the material behaviour. Consequently, the fatigue life prediction model needs to be based on creep deformation [46]. According to various mechanical parameters, fatigue life prediction models of solder interconnect can be classified into five classes: based on energy, plastic strain, creep strain, stress, and cumulative damage.

A. Solder Fatigue Life Assessment

Solder joint fatigue phenomenon on lead-free solder interconnects have been a subject of numerous studies. Failure in low-cycle fatigue (LCF) is mainly as a result of cyclic plastic deformation. When a solder interconnection is loaded, the stress-strain curve would be a linear plot with an elastic behaviour until the yield point. Studies has shown that LCF is associated with shorter fatigue life and higher stress where the stress level usually steps into the plastic strain range. The Coffin-Manson which has been widely used to predict the LCF as a function of plastic strain range for solder alloys has been applied to predict the fatigue life of the solder alloys considered in this study. The Engelmaier model modified the Coffin-Manson model by including parameters such as solder and substrate temperature into the equation identified as Engelmaier model [47] as presented in equation 1. Failure in low-cycle fatigue is mainly due to plastic deformation. The Engelmaier model is the correction of Coffin-Manson model [48]–[51]. This model takes the temperature and frequency into account making it easier to get a more precise result. The relationship is presented in equation 1 and the value of c is obtained from equation 2 [43].

$$N_f = \frac{1}{2}\left(\frac{\Delta\gamma}{2\varepsilon_f'}\right)^{\frac{1}{c}} \quad (1)$$

Where N_f is the mean cycle to failure, $\Delta\gamma$ is the cyclic shear strain range, ε_f' is the fatigue ductility coefficient [$2\varepsilon_f' = 0.65$ lead-based eutectic solder alloys and $2\varepsilon_f' = 0.48$ for SAC solder alloy materials [52] and *c* is the fatigue ductility exponent (c = -0.442 for eutectic and 0.5708 for SAC solder alloys).

When solder joints are at high extreme temperature, creep failure dominates; and when exposed to temperature cycling, fatigue failure dominates [13]–[20], [43]. If under the combination of both, the failure mechanism is generally referred to as creep-fatigue [21], [53]. The creep and fatigue of solder joints are primarily due to the mismatch of coefficient of thermal extension (CTE) between electronics component and PCB. Low-cycle fatigue (LCF) is associated with shorter fatigue life and higher stress where stress level usually steps into the plastic strain range. Coffin-Manson model equation [54] is widely used to predict the low-cycle fatigue life N_f as a function of plastic strain range $\Delta\varepsilon_p$ for solder alloys:

$$N_f^m \Delta\varepsilon_p = C \quad (2)$$

where $m = 0.70$ is the fatigue exponent and $C = 1.69$ is the ductility coefficient for eutectic solder alloy [55].

Solomon proposed a low-cycle fatigue model (Equation 3) that relates the plastic shear strain to the fatigue life cycles for near eutectic solder joints at four different temperatures $-50℃, 35℃, 125℃$ and $150℃$ [56], [57].

$$\Delta\gamma_p N_f^{\alpha} = \theta \quad (3)$$

where $\Delta\gamma_p$ is the plastic shear strain range and α and θ are constants. For 60/40 Tin-lead solder material from $-50℃$ to $150℃$, α and θ are estimated to be 0.51 and 1.14 respectively [43], [58].

B. Anand Model Equations

Anand model contains both time-dependent plastic and viscoplastic phenomenon where growth of plastic strain is dependent on the rate of loading [59], [60]. Viscoplastic on

the other hand is described by unifying creep and plastic deformations [61]. Anand's model is utilised in situations where the material behaviour is particularly susceptible to temperature, strain rate, history of temperature and strain rate, and strain softening and hardening. The model has proved for application in predicting the response and life of solder interconnect in electronic devices and packaging.

The Anand's model proposes a singular scalar quantity described as the deformation resistance, which is employed to characterise the isotropic resistance to the inelastic flow of the material. The comparison of the inelastic strain rate is presented in equation 4:

$$\bar{\sigma} = cs; c < 1 \quad (4)$$

where $\bar{\sigma}$ the equivalent stress for steady plastic flow; s is the deformation resistance with the dimensions of stress. c is a function of strain rate and temperature as expressed as:

$$c = \frac{1}{\xi} sinh^{-1}\left\{\left(\frac{\dot{\varepsilon}^p}{A} exp\left[\frac{Q}{RT}\right]\right)^m\right\} \quad (5)$$

Combining equation 4 & 5

The Anand model uses the following functional form to describe the flow equation as:

$$\dot{\varepsilon}^p = A\exp\left(-\frac{Q}{RT}\right)\left(sinh\left[\xi\frac{\bar{\sigma}}{s}\right]\right)^{\frac{1}{m}} \quad (6)$$

where $\dot{\varepsilon}^p$ is the inelastic strain rate; A is pre-exponential factor; Q is the activation energy; R is universal constant; T is the temperature; R is universal gas constant; T is the temperature; ξ stands for the materials constant and m is the strain rate sensitivity.

Additionally, the evolution equation for the internal variable s is assumed to be in the form as:

$$\dot{s} = h(\bar{\sigma}, s, T)\dot{\varepsilon}^p \quad (7)$$

$h(\bar{\sigma}, s, T)$ is associated with dynamic strain hardening and recovery process. A simple form of evolution equation of equation 7 was given by Anand as follows [59]:

where

$$h = h_0\left|1 - \frac{s}{s^*}\right|^a sign\left(1 - \frac{s}{s^*}\right) \qquad a \geq 1 \quad (8)$$

Therefore, the evolution equation for the internal variable s is derived from combined form of equation 7 & 8 as:

$$s = \left\{h_0\left|1 - \frac{s}{s^*}\right|^a sign\left(1 - \frac{s}{s^*}\right)\right\}\dot{\varepsilon}^p \quad (9)$$

where

$$s^* = \hat{s}\left(\frac{\dot{\varepsilon}^p}{A} exp\left[\frac{Q}{RT}\right]\right)^n \quad (10)$$

where s^* describes the saturation value of *s* associated with a set of given temperature and strain rate; h_0 represents the hardening/softening constant; a is the strain rate sensitivity of hardening/softening; *n* stands for the strain rate sensitivity for the saturation value of deformation resistance, and $\hat{s}$ is a coefficient.

The viscoplastic model comprises of two types of equations. The first equation deals with the correlation between saturation strain and stress rate under specific temperature. In contrast, the second equation deals with the relationship between strain and stress under particular temperature and strain rate [98].

III. METHODOLOGY

A. Thermal Cycling Test

A1. Convergence and Mesh Independence Study

The formal process of determining mesh convergence requires a curve of a critical result parameter deformation and stress plotted against the mesh density. Solder materials are susceptible to significant creep deformations in harsh high-temperature environments such as oil exploration, automotive, avionics, and military applications. Also, degradations will happen in the creep responses of lead-free solder alloys when they are exposed to long-term thermal ageing during product applications at high temperatures. The following necessary steps are needed to perform a mesh convergence study: (1) Generate a mesh utilising the fewest, moderate quantity of elements and examine the model; (2) Recreate the mesh with a denser element configuration, re-analyse it, and analyse the outcomes to those of the earlier mesh; (3) Continue increasing the mesh density and re-analysing the model until the results converge adequately to a solution.

A2. Basic Assumptions and Analysis Methodologies

- The material property of the solder bump is nonlinear and temperature dependent. In other words, others are linear and temperature independent.
- Every interface of the materials is assumed to be in contact with each other totally.
- All the materials were modelled as linear elastic and isotropic materials except the solder and PCB which are simulated using the Anand's model relations and orthographic materials respectively.
- All materials including the solder joint were assumed homogeneous at load steps.
- The initial stress in the assemblies which may be accumulated from reflow soldering process is neglected, and all contacting surfaces are assumed to be bonded with perfect adhesion

A3. Geometrical and Mesh Models

The BGA package includes solder ball, Silicon (Si), die substrate, Copper (Cu) pad and epoxy-resin (FR-4). The parameters and package dimensions of the lead-free solder BGA are shown in the author's other publications Depiver et al. [62], [63]. The necessity to use a quarter of the full model is to reduce simulation solve time and processes since the aim of the research is to investigate BGA solder joint in the package for thermo-mechanical reliability. It also augments operational test design and evaluation because the full assembly is big and complex; much time is needed to complete a simulation; therefore, a quarter symmetry is perfect for running several simulations.

A4. Material Properties and Parameters

Except for the PCB, the properties of all other materials are linear and temperature dependent. The material properties used are obtained from several works of literature. The critical materials used in the assembly in mounting the BGA on PCB are solder alloys, copper pad, epoxy-resin (FR-4), solder mask and Silicon (Si) die. All the materials were modelled as linear elastic and isotropic substances except the PCB and the solder alloys, which was simulated using the orthographic materials and Anand models respectively. The material properties used

for the FEA simulation experiments is presented in Table 1 and 2.

TABLE 1: Materials properties for the BGA on PCB Components

Materials	Reference	Young's Modulus (GPa)			C.T.E (ppm/°C)			Poisson's Ratio		
		E_x	E_y	E_z	α_x	α_y	α_z	v_{xy}	v_{xz}	v_{yz}
Silicon (Si) Die	[64]	110.0			2.60			0.24		
PCB Mask	[65]	4.14			30.0			0.40		
Cu Pad	[66]	129.0			17.0			0.34		
PCB	[67]	27.0	27.0	22.0	14.0	14.0	15.0	0.17	0.20	0.17
Epoxy-Resin (FR-4)	[64]	29.9	25.1	70.0	12.0	15.0		0.16	0.14	
Sn63Pb37	[68]	56.0			20.0			0.30		
SAC305	[64]	51.0			23.5			0.40		
SAC387	[69]	45.0			17.6			0.36		
SAC396	[70]	43.0			23.2			0.30		
SAC405	[71]	44.6			20.0			0.42		

TABLE 2: Anand model constant for eutectic lead-based Sn63Pb37 and lead-free SAC305, SAC387, SAC396 and SAC405 solder alloys

	Solder				
Anand Parameters	**Sn63Pb37** [72]	**SAC305** [73]	**SAC405** [74]	**SAC387** [75]	**SAC396** [76]
$\mathbf{s_o}$ **(MPa)**	3.1522	45.9	20.0	39.5	3.3
$Q/R\,(K^{-1})$	6,526	7,460	10,561	8,710	9,883
A (s^{-1})	6,220	5.87×10^6	325	24,300	1.57×10^7
ξ	3.33	2.00	10.00	5.8	1.06
m	0.27	0.0942	0.32	0.183	0.3686
$\mathbf{h_o}$ **(MPa)**	60,599	9,350	8×10^5	3,541.2	1077
$\hat{s}$ **(MPa)**	36.86	58.3	42.0	65.3	3.15
n	0.022	0.015	0.02	0.019	0.0352
a	1.7811	1.5	2.57	1.9	1.6832

A5. Loading and Boundary Conditions

In applying the FE Analysis for the thermal cycling analysis, the ambient temperature cycle is external loading. The FE models were subjected to six complete ATC's in 36 steps shown in Fig. 10. The thermal cycling temperature is from -40℃ to +150℃ with 15℃/min ramp, and 5mins dwell based on IEC 60749-25 temperature cycling and JEDEC Standard JESD22-A104D [77]–[79] shown in Fig. 1 was used. The quarter assembly components were first heated from room temperature 22℃ which is the starting temperature in thermal cycle loading with constant heating rate. They are also assumed to be at a homologous temperature at loads steps. The temperature loading started from 22℃, dwelled at -40℃ at the rate of 15℃/min, and ramped up to 22℃ for the 23 mins and excursion temperature (ET) of 150℃ for 31.8 mins where it dwelled for 5 mins. Applications used for this profile are the automotive under-hood, semiconductors in power supply controllers and military. The assemblies were supported such that the conditions of the structure at the supports are:

At the PCB base, $y = 0$, and $u_{(y)} = 0$;

Top surface $u_{(y)} = 0$, $u_{(x)}$ and $u_{(z)}$ are free.

The $u_{(x)}$, $u_{(y)}$ and $u_{(z)}$ represents the displacement in the x, y and z directions respectively. The bottom surface of the PCB was fixed in Y direction and displaced in the X and Z directions.

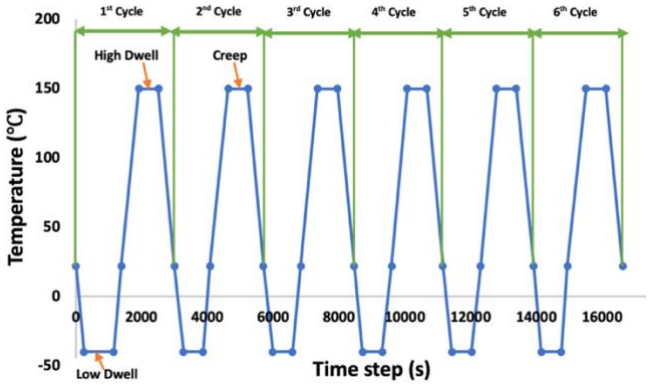

Fig. 1: Thermal Cycling temperatures boundary profile

B. Failure Criterion

The generally used solder-joint failure criteria include those based on classic fracture mechanics [8], plastic strain [54], [80]–[82], creep strain [83]–[86], fracture-calibrated energy [87] and inelastic work [88], [89]. For experimental failure studies, resistance is also used as failure criteria. Each failure criterion requires specific material properties and may place the requirements on the nature of the numerical solution obtained either by computation or through FEA simulation. For this investigation, the failure criterion is based on maximum plastic strain values from FEA simulation. This is then used in the Engelmaier, Coffin-Manson and Solomon models' calculations to obtain the fatigue life characteristics of the five solder joint alloy materials (lead-based eutectic Sn63Pb37, and lead-free SAC305, SAC387, SAC396 and SAC405) used in this study.

RESULTS AND DISCUSSIONS

C. Thermal Cycling Results of Solder Joints

The simulation results for lead-based eutectic Sn63Pb37 and four SAC (SAC305, SAC387, SAC396 and SAC405) solder alloy materials used in this work are presented. The results reveal that thermal stresses were produced in the solder joints during thermal processes. FEA was employed in the investigation of the solder joints to ascertain the reliability

of during thermal cycling. The study on the constitutive model of the solder joints can yield the data support for the reliability study. Anand model, which is a unique built-in material model in the FE programs in ANSYS, was adopted to obtain the stress, strain, strain energy and deformation distribution of solder joints in electronic packaging. The material properties and parameters of the Anand model for the eutectic Sn63Pb37 and SAC solder joints were obtained from published literature.

Additionally, based on the Anand model, FE was used to examine its reliability during thermal cycling. The simulated result presented reveals a cross-section of the failed bumps. Cracks are understood to produce at the top corners of the solder joint in the substrates. Furthermore, the residual stress effect during simulation has influences on the strains during temperature cycling, which adds to the fatigue life model prediction results.

A1. Effects of Plastic Strain

Five types of solders were simulated in this study. FE software ANSYS R19.0 was used to simulate solder joints to determine their fatigue failure and reliability. The results obtained imply that plastic deformation of solder joint due to thermal cycle loading can be used in predicting the fatigue life of solder joints. The plot in Fig. 2 shows that SAC387 and SAC305 have the highest plastic strain why SAC405 and SAC396 with the lowest plastic strain which indicates that the fatigue life of SAC387 is lower than the rest of the solder joints examined. The fatigue life of the solder joints is calculated using the modified Coffin-Manson, Solomon and Engelmaier equation based on FE simulation. The results show that lead-based eutectic Sn63Pb37 has a plastic strain of 0.0104 why the SAC305, SAC387, SAC396 and SAC405 has the following strain values of 0.0055, 0.0247, 0.0091 and 0.0076, respectively. The fatigue life of SAC405 is higher than that of the other four solders joints reflecting the increase of the fatigue resistance in the solder joint to some extent and changes in the crack's propagation during the fracture process. As mentioned earlier, the modified fatigue life equation was used for estimating the useful lifetime of the solder joints because they are still the most convenient tool employed in the calculation of thermal fatigue life of solder joints. The fatigue life of lead-based eutectic Sn63Pb37 and lead-free SAC (SAC305, SAC387, SAC396 and SAC405) solder joints are presented in Table 3. More details of fatigue life estimation are described in section II. Fig. 3 shows the schematic trend of the maximum plastic strain of solder interconnects. During dwell time, the plastic strain change results from the creep of solder or induced fatigue cracks.

A2. Effect of Von Mises Stress

The effects of Von mises stress on the thermal cycling of solder joints is present in Figs. 4 and 5. The chart (Fig. 4) shows that SAC396 followed by the lead-based eutectic Sn63Pb37 has the lowest Von mises stress magnitude in comparison with the high-stress values obtained for SAC405 and SAC387. The stress values for SAC396 obtained is 9.22MPa why the highest stress magnitude for SAC405 and SAC387 were 38.72MPa and 36.38MPa, respectively. The other solders which are the lead-based eutectic Sn63Pb37 and SAC305 have a stress magnitude value of 15.38MPa and 22.07MPa respectively. The impact of stress on the performance of the BGA electronics component is as a result of thermal and mechanical variations. As it could be seen in Fig. 5, the highest stress is understood to have occurred at the corners of the SAC396 solder joints arrangements. The effects of IMC were examined in subsequent work. The simulation results obtained, along with experimental results obtained from several works of literature, are very important to access test data and prevents early fatigue failures in BGA electronic devices.

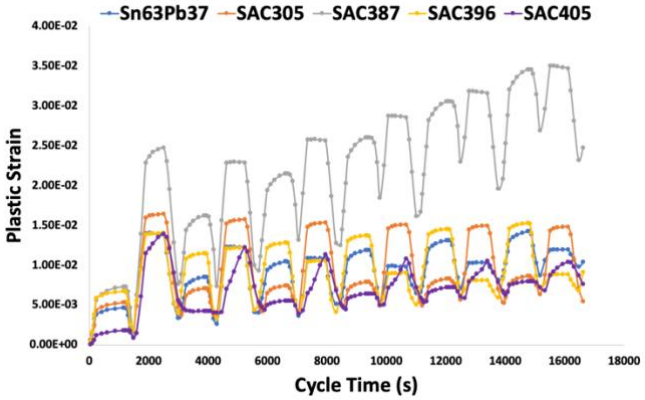

Fig. 2: Plot of plastic strain rate for lead-based eutectic Sn63Pb37 and lead-free SAC305, SAC387, SAC396, and SAC405 solder alloy materials

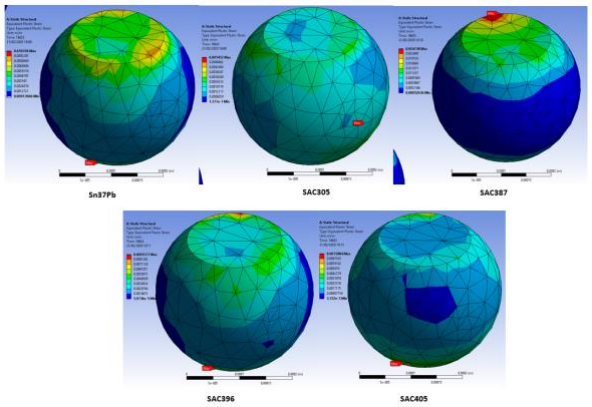

Fig. 3: Schematics for lead-based eutectic Sn63Pb37 and lead-free SAC305, SAC387, SAC396 and SAC405 showing areas of maximum plastic strain

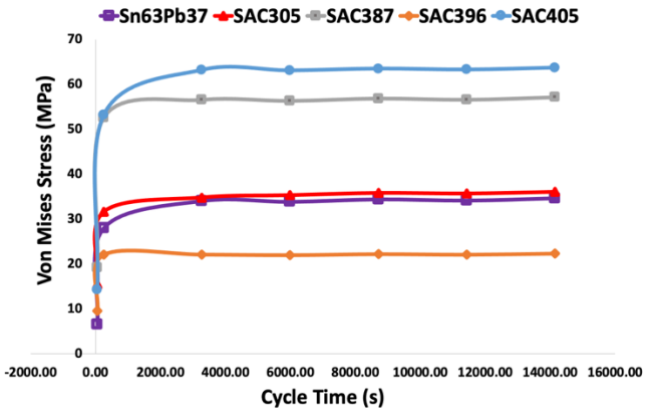

Fig. 4: Von Mises stress results for six complete cycles of solder alloys

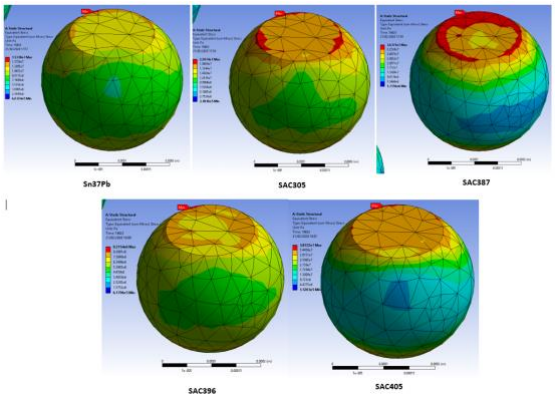

Fig. 5: Schematics for lead-based eutectic Sn63Pb37 and lead-free SAC305, SAC387, SAC396 and SAC405 showing areas of maximum Von mises stress on solder joints

A3. Effect of Deformation Rate

The deformation rates on various solder joints considered in this work are shown in Figs. 6 and 7. The results show that SAC305 ($0.381\mu m$), SAC396 ($0.429\mu m$) and SAC405 ($0.452\mu m$) has the lowest deformation rates compared to SAC387 ($0.803\mu m$) and eutectic Sn63Pb37 ($0.458\mu m$) having the highest deformation rates. These data obtained along with creep exponents, strain rate sensitivities and damage mechanisms are valuable in supporting the modelling of solder joints for reliability and lifetime prediction.

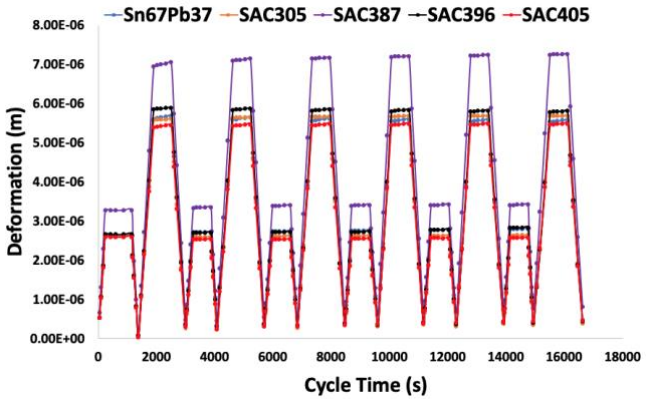

Fig. 6: Deformation rate results of six cycles of solder alloys

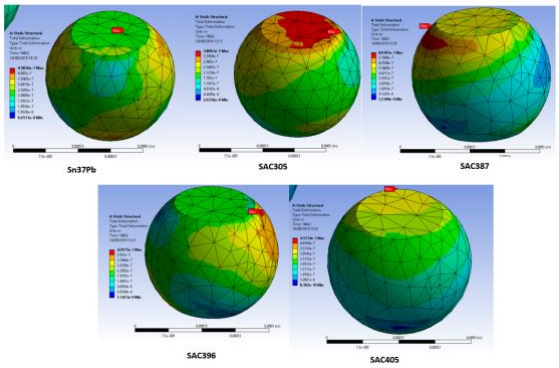

Fig. 7: Schematics for lead-based eutectic Sn63Pb37 and lead-free SAC305, SAC387, SAC396 and SAC405 showing areas of maximum deformation on solder joints

A4. Effect of Strain Energy Density

The FEA results showing the strain energy density results are presented in Figs. 8 and 9. The results show that among the five solders considered in the FE simulation, SAC387 ($0.0101\mu m$) and SAC396 ($0.022\mu m$) has the lowest strain energy density why SAC305 ($0.047\mu m$), SAC405 ($0.041\mu m$) and eutectic Sn63Pb37 ($0.035\mu m$) has the highest strain energy density dissipated on the solder joints. The critical value of the strain energy density represents the intrinsic property of solder. The result demonstrates the applicability of the strain energy density for the reliability life prediction of solder joints. In cases reported here, solder joints failed at the package interface. The result is in agreement with experimental results by Syed [85] for SnAgCu solder alloy and is presented in Fig. 10. SAC396 and SAC405 offer the best alternative for lead-free SAC and lead-based eutectic Sn63Pb37 solders currently in use. With the current trend of cheaper, faster, and better electronic devices, it has become increasingly important to evaluate the package and system performance very early in the design cycle stage using simulation tools such as ANSYS and selecting the right solder alloy is essential.

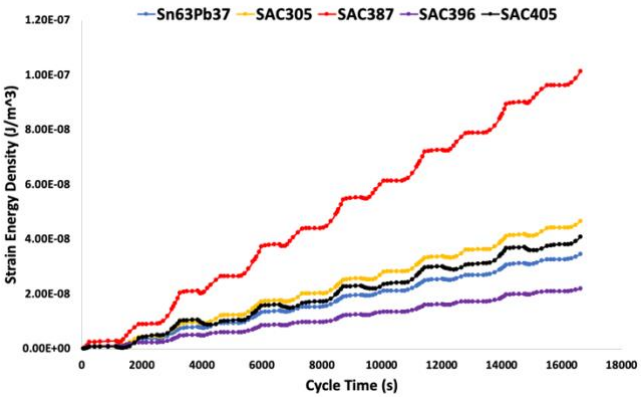

Fig. 8: Strain energy density thermal cycle results for solders

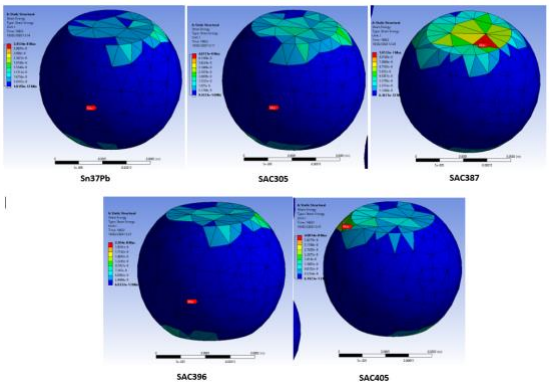

Fig. 9: Schematic representations for lead-based eutectic Sn63Pb37 and lead-free SAC305, SAC387, SAC396 and SAC405 showing areas of maximum strain energy on solder joints

Experimental studies conducted by Tong An et al., [90] who investigated the failure study of Sn63Pb37 PBGA solder joints using temperature cycling, random vibration and combined temperature cycling and random vibration tests. A thermal cycling ($-55℃$ to $125℃$) and vibration studies were carried out for eutectic lead-based Sn63Pb37 solder joint. The findings from their work demonstrate that earlier solder joint failure for combined loading than that for either temperature cycling or pure vibration loading at room temperature. The primary failure mode is cracking within the bulk solder under temperature cycling, whereas the crack

propagation path is along with the intermetallic compound (IMC) layer for vibration loading. Fig. 10 shows a typical failure mode when the components are subjected to thermal cycling loading. The results suggest that most of the cracks in the failed solder joints were located on the component side. The primary failure mode is a fracture within the bulk solder (where the crack initiates and propagates within the bulk solder). During thermal cycling, the solder joint experiences alternating stresses during the heating and cooling duration and this induces accumulated plastic deformation and causes the cracks to open especially because the inelastic strain is highest at near the Silicon die thereby the solder joint failed at this critical solder joint and failure occurs.

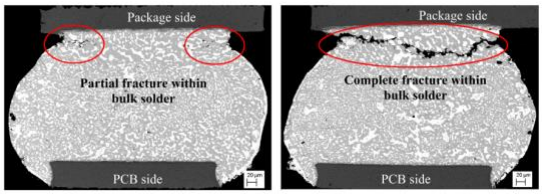

Fig. 10: SEM image of solder joint failure modes of the solder joints during temperature cycling showing cracked at component interface of eutectic 63Sn37Pb solder [90]

Hsieh and Tzeng [91] investigated the solder joint fatigue life prediction in large size and low-cost wafer-level chip-scale packages. They assessed the fatigue life of considerable size and low-cost WLCSP with SAC105 solder joints, the board level reliability (BLR) thermal cycling test that follows JEDEC models. The failure consequences of SAC105 in BLR thermal cycling test is for 185, and 188 cycles are presented in Fig. 11. In conclusion, a modified Coffin-Manson equation for SAC105 solder joint fatigue life was achieved. With the existing equations, the solder joint fatigue life in a large size and low-cost WLCSP can be determined by simulations without works on experimental evaluations. The outcomes achieved are relevant and beneficial if high reliability and cost reduction in large die size and low-cost WLCSP are needed. By examining the SEM images, it was determined that the solder crack initially occurred near the corner of the pad and solder ball. The solder crack propagated along at the top IMC layer underneath the pad as well as along the top surface of the PCB Cu pad in the WLCSP. Similarly, Mi [92] reported a crack in the corner of the BGA side, as shown in Fig. 12.

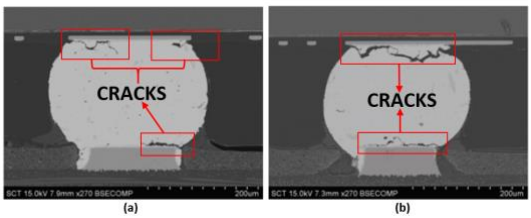

Fig. 11: Failure results of SAC105 solder joint in board level reliability (BLR) thermal cycling test (TCT) in test vehicle (a) larger redistribution layer (RDL) pad size and (b) smaller redistribution layer (RDL) pad size [91]

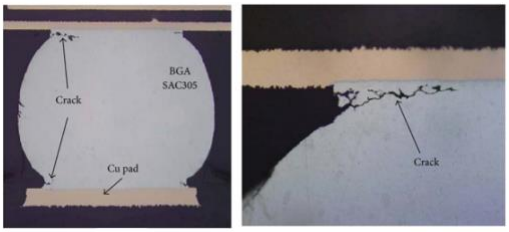

Fig. 12: Crack image after 2500 thermal cycles. (a) A complete solder joint and (b) a corner of BGA side [92]

Similarly, work carried out by George et al. [93] on the thermal cycling reliability of lead-free solders (SAC305 and Sn3.5Ag) for high-temperature applications shows similar deformation results (Fig. 13). In their research, ball grid arrays (BGA), quad flat packages (QFP), and surface mount resistors assembled with SAC305 and Sn3.5Ag solder pastes were subjected to thermal cycling from −40℃ to 185℃. The result of their work shows that the failure was concentrated on the package side of the solder joint, which is comparable to results obtained from our FEA. Several researchers such as Xie et al., [94] has reported a crack in the same location except in certain conditions that fatigue failure is observed on the PCB side of the component. Other investigation by [95]–[99] also reported the same crack location on the components section of the electronics package. Another typical failed SnAgCu solder joint cross-section was reported by Syed [46] presented in Fig. 14

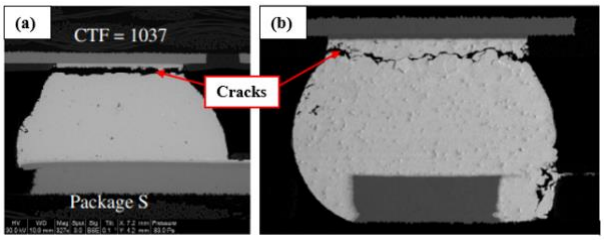

Fig. 13: SEM image of a solder joint cracked at interface of solder and IMC at die side after being subjected to accelerated thermal cycling: (a) adapted package side crack on 144 I/O BGA (Sn based finish SAC305 solder) (b) adapted cracked joint [93]

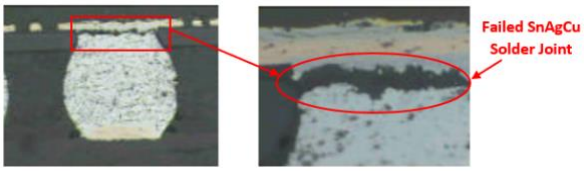

Fig. 14: Typical failed SnAgCu solder joint cross-section [Adapted Ref. [46]]

A5. Analysis of Stress-Strain Hysteresis loop

During thermal loading, the area under the stress-strain curve is the strain energy per unit volume absorbed by the solder alloy materials. On the other hand, the area under the unloading curve is the energy released by the solder alloy materials. During the elastic range, these areas are equal, and no net energy is absorbed. If the material is loaded in plastic range as presented in Fig., the energy consumed surpasses the energy discharged, and the difference between them is dispelled as heat. Perfect elastic materials possess an ideal linear stress-strain characteristic. Cyclic stress produces a strain in the solder materials, which is a cyclical variable and

in phase with the stress. Solder joint cracking is inhibited in loading since cracks will be closed instead opened by the stress state. The solder materials loaded cyclically to alternate between loading and unloading can exhibit hysteresis loops since the load is high enough to induce plastic flow (stresses above the yield stress). The area of the surface enclosed within the hysteresis loop always equals the amount of energy dissipated in the material upon the loading-unloading cycle. On the contrary, the hysteresis loop yield information on fatigue degree, as well as a stress-strain characteristics curve. This demonstrates that the solder materials stress variations result with an increase of fatigue degree and a reduction of mechanical strength.

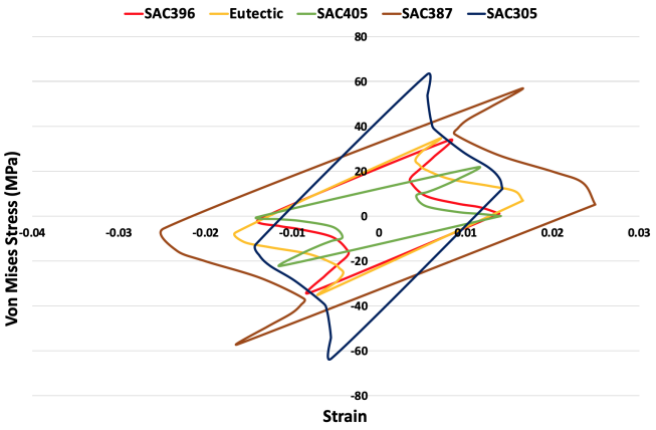

Fig. 16: Stress-strain hysteresis loop for lead-based eutectic Sn63Pb37 and lead-free SAC305, SAC387, SAC396 and SAC396 solder alloys

A6. Analysis of Thermal Fatigue Life of BGA Solder Joints based on Engelmaier, Coffin-Manson and Solomon Models

The thermal fatigue life of a solder joint has become a critical factor in the reliability of electronics products. Several life predictions models have been proposed and are mainly obtained by associating stress, strain and strain energy density. The fatigue life model can be divided into five categories, namely stress, strain, creep strain, energy and cumulative damage. The section employs life prediction model of solder joints under thermal cycling, the Engelmaier, Coffin-Manson and Solomon model are accompanied by plastic strain during low cycle fatigue thus the Basquin damage model is not a good fit for life prediction model based on plastic deformation.

Engelmaier model is widely used to calculate the fatigue life of solder joints in microelectronic devices subjected to thermal cycling loading conditions. Finite element analysis was conducted on the BGA on PCB samples of eutectic Sn63Pb37, SAC305, SAC387, SAC396 and SAC405 to obtain the failure time and comparing the fatigue lives of the solder alloy materials. The plots presented in Figs. 17 and 18 show the number of cycles to failure and number of years to failure of solder interconnects. The parameters such as plastic strain, plastic shear strain and used in the calculation are extracted directly from ANSYS why the constants are derived from several experimental results obtained by numerous investigators from literature. From the results obtained, SAC405 has the highest fatigue life to failure under the Engelmaier, Coffin-Manson and Solomon models followed by SAC396 and SAC305 solders. From the investigations conducted so far, it can be concluded that SAC's simulation-based prediction of fatigue life indicates that SAC405 followed by SAC396 are the preferred solder joint alloy materials for the replacement of eutectic lead-based alloy for enhanced thermo-mechanical reliability of solder joints. The results corroborate well with the work by Syed [85] whose mean life covers a range of data from 275 cycles to 10027 cycles for SAC solder and 416 cycles to 5953 cycles for SnPb solder joints. The results of this work show that SAC405 and SAC396 solder joints had higher reliability than the eutectic Sn63Pb37, SAC387, and SAC305 solder interconnect. The strain-based models are fit for fatigue prediction for low-cycle fatigue, while the stress-based models are generally employed to predict high-cycle fatigue. Most of the fatigue models predict the number of cycles to failure.

TABLE 3: Number of cycles to failure for eutectic Sn63Pb37, SAC305, SAC387, SAC396 and SAC405 solder alloy materials

Solder	Engelmaier	Coffin-Manson	Solomon
Sn63Pb37	4948	1477	3448
SAC305	11075	9917	11820
SAC387	2439	1119	1906
SAC396	13625	14850	13075
SAC405	18738	15359	13967

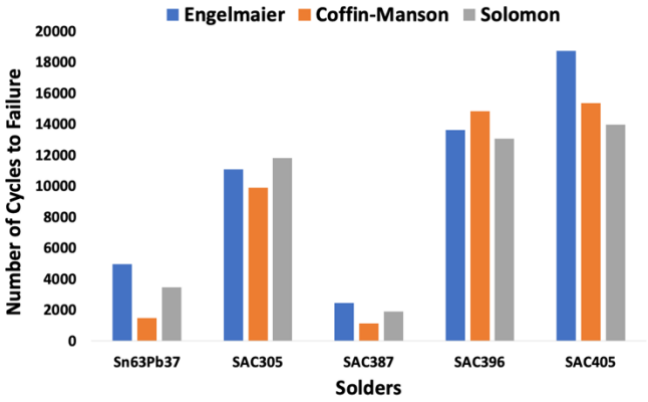

Fig. 17: Plot of number of cycles to failure for eutectic Sn63Pb37, SAC305, SAC387, SAC396 and SAC405 solder alloy materials

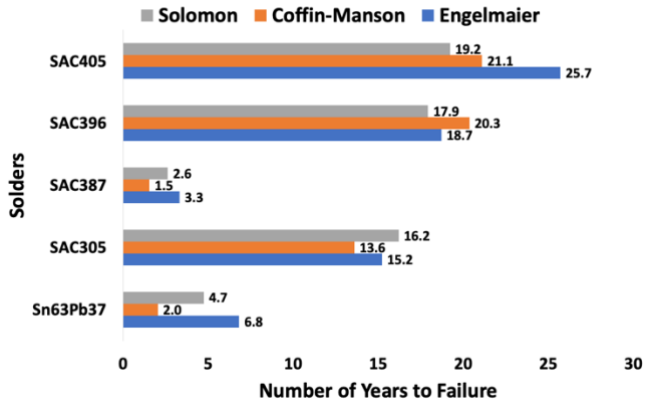

Fig. 18: Plot of number of years to failure for eutectic Sn63Pb37, SAC305, SAC387, SAC396 and SAC405 solder alloy materials

IV. CONCLUSION

In this paper, the reliability of solder joints was analysed with thermal cycle loading to predict the fatigue life of eutectic Sn63Pb37, SAC305, SAC387, SAC396 and SAC405 using the Solomon, Coffin-Manson and Engelmaier models

as the basis of comparison. The result shows that SAC405 and SAC396 possesses a longer fatigue life across the three models investigated. It is also shown that the minimum stress magnitude and strain were observed on the SAC405 and SAC396 solder joints, respectively, which is at the top of the BGA solder joints device edge. Accordingly, the study evaluated the stress-strain hysteresis response indicating that SAC405 followed by SAC396 has the lowest dissipated energy. Based on the results obtained, there were noticeable distinguishing features on the three models considered in this work. The work proposed the use of Engelmaier (total shear strain), Coffin-Manson (plastic strain) and Solomon (plastic shear strain) model in that particular order in a low cycle fatigue coverage by electronic manufacturing engineers when considering the best BGA solder alloy materials with the maximum years to failure in a thermo-mechanical loading environment.

Acknowledgment

The work reported in part in this article is funded by the School of Mechanical Engineering & the Built Environment, College of Engineering & Technology, University of Derby, UK.

REFERENCES

[1] L. Zhang and K. N. Tu, "Structure and properties of lead-free solders bearing micro and nano particles," *Materials Science and Engineering R: Reports*. 2014.

[2] K. Kanlayasiri and K. Sukpimai, "Effects of indium on the intermetallic layer between low-Ag SAC0307-xIn lead-free solders and Cu substrate," *J. Alloys Compd.*, 2016.

[3] R. J. Coyle, K. Sweatman, and B. Arfaei, "Thermal Fatigue Evaluation of Pb-Free Solder Joints: Results, Lessons Learned, and Future Trends," *JOM*, vol. 67, no. 10, pp. 2394–2415, 2015.

[4] R. Schueller *et al.*, "Second Generation Pb-Free Alloys," 2003.

[5] W. J. Plumbridge, "Second generation lead-free solder alloys - A challenge to thermodynamics," in *Monatshefte fur Chemie*, 2005.

[6] F. Ji, S. Xue, L. Zhang, L. Gao, Z. Sheng, and W. Dai, "Reliability evaluation of QFN devices soldered joints with creep model," *Chinese J. Mech. Eng. (English Ed.*, 2011.

[7] L. Sun, L. Zhang, S. juan Zhong, J. Ma, and L. Bao, "Reliability study of industry Sn3.0Ag0.5Cu/Cu lead-free soldered joints in electronic packaging," *J. Mater. Sci. Mater. Electron.*, vol. 26, no. 11, pp. 9164–9170, 2015.

[8] J. H. Lau and Y. Pao, *Solder joint reliability of BGA, CSP, Flip Cip, and fine pitch SMT assemblies*. 1997.

[9] Lau John; Wong C P; Lee Ning-Cheng, *Electronics Manufacturing: With Lead-Free, Halogen-Free, and Conductive-Adhesive Materials*. The McGraw-Hill Companies, Inc., 2003.

[10] J. Wang, Y. Niu, S. Park, and A. Yatskov, "Modeling and design of 2.5D package with mitigated warpage and enhanced thermo-mechanical reliability," in *Proceedings - Electronic Components and Technology Conference*, 2018.

[11] S. Shao *et al.*, "Comprehensive study on 2.5D package design for board-level reliability in thermal cycling and power cycling," in *Proceedings - Electronic Components and Technology Conference*, 2018.

[12] X. C. Tong, "Thermal Management Fundamentals and Design Guides in Electronic Packaging," 2011.

[13] S. Hamasha, A. Qasaimeh, Y. Jaradat, and P. Borgesen, "Correlation Between Solder Joint Fatigue Life and Accumulated Work in Isothermal Cycling," *IEEE Trans. Components, Packag. Manuf. Technol.*, 2015.

[14] A. Qasaimeh, S. Hamasha, Y. Jaradat, and P. Borgesen, "Damage evolution in lead free solder joints in isothermal fatigue," *J. Electron. Packag. Trans. ASME*, 2015.

[15] M. Obaidat *et al.*, "Effects of varying amplitudes on the fatigue life of lead free solder joints," in *Proceedings - Electronic Components and Technology Conference*, 2013.

[16] F. Batieha, S. Hamasha, Y. Jaradat, L. Wentlent, A. Qasaimeh, and P. Borgesen, "Challenges for the prediction of solder joint life in long term vibration," in *Proceedings - Electronic Components and Technology Conference*, 2015.

[17] P. Borgesen *et al.*, "A Mechanistic Thermal Fatigue Model for SnAgCu Solder Joints," *J. Electron. Mater.*, vol. 47, no. 5, pp. 2526–2544, 2018.

[18] S. Hamasha and P. Borgesen, "Effects of strain rate and amplitude variations on solder joint fatigue life in isothermal cycling," *J. Electron. Packag. Trans. ASME*, 2016.

[19] S. Hamasha, S. Su, F. Akkara, A. Dawahdeh, P. Borgesen, and A. Qasaimeh, "Solder joint reliability in isothermal varying load cycling," in *Proceedings of the 16th InterSociety Conference on Thermal and Thermomechanical Phenomena in Electronic Systems, ITherm 2017*, 2017, pp. 1331–1336.

[20] S. Su, M. Jian, F. J. Akkara, S. Hamasha, J. Suhling, and P. Lall, "Fatigue And Shear Properties Of High Reliable Solder Joints For Harsh Applications Department of Industrial and Systems Engineering Department of Mechanical Engineering," 2018.

[21] H. U. Akay, N. H. Paydar, and A. Bilgic, "Fatigue life predictions for thermally loaded solder joints using a volume-weighted averaging technique," *J. Electron. Packag. Trans. ASME*, 1997.

[22] W. B. Green, "A fatigue-free silicon device structure," *Trans. Am. Inst. Electr. Eng. Part I Commun. Electron.*, vol. 80, no. 2, pp. 186–192, 2013.

[23] T. Y. Tee, H. S. Ng, D. Yap, X. Baraton, and Z. Zhong, "Board level solder joint reliability modeling and testing of TFBGA packages for telecommunication applications," in *Microelectronics Reliability*, 2003.

[24] A. Schubert *et al.*, "Reliability assessment of flip-chip assemblies with lead-free solder joints," *Proc. - Electron. Components Technol. Conf.*, 2002.

[25] W. D. Zhuang, P. C. Chang, F. Y. Chou, and R. K. Shiue, "Effect of solder creep on the reliability of large area die attachment," *Microelectron. Reliab.*, 2001.

[26] T. Y. Tee, H. S. Ng, and Z. Zhong, "Board level solder joint reliability analysis of stacked die mixed flip-chip and wirebond BGA," *Microelectron. Reliab.*, 2006.

[27] S. Park, R. Dhakal, L. Lehman, and E. Cotts, "Measurement of deformations in SnAgCu solder interconnects under in situ thermal loading," *Acta Mater.*, 2007.

[28] J. C. Suhling *et al.*, "Thermal cycling reliability of lead free solders for automotive applications," in *Thermomechanical Phenomena in Electronic Systems -Proceedings of the Intersociety Conference*, 2004.

[29] J. S. Hwang and R. M. Vargas, "Solder joint reliability—can solder creep?," *Solder. Surf. Mt. Technol.*, vol. 2, no. 2, pp. 38–45, 1990.

[30] C. Huang, D. Yang, B. Wu, L. Liang, and Y. Yang, "Failure mode of SAC305 lead-free solder joint under thermal stress," in *ICEPT-HDP 2012 Proceedings - 2012 13th International Conference on Electronic Packaging Technology and High Density Packaging*, 2012.

[31] J. H. L. Pang, D. Y. R. Chong, and T. H. Low, "Thermal cycling analysis of flip-chip solder joint reliability," *IEEE Trans. Components Packag. Technol.*, 2001.

[32] A. Choubey, M. Osterman, and M. Pecht, "Microstructure and intermetallic formation in SnAgCu BGA components attached with SnPb solder under isothermal aging," *IEEE Trans. Device Mater. Reliab.*, vol. 8, no. 1, pp. 160–166, 2008.

[33] T. C. Chiu, K. Zeng, R. Stierman, D. Edwards, and K. Ano, "Effect of thermal aging on board level drop reliability for Pb-free BGA packages," in *Proceedings - Electronic Components and Technology Conference*, 2004.

[34] H. Ma, J. C. Suhling, P. Lall, and M. J. Bozack, "Reliability of the aging lead free solder joint," in *Proceedings - Electronic Components and Technology Conference*, 2006.

[35] J. Zhang, Z. Hai, J. L. Evans, M. J, J. C, and A. Silver, "Correlation of aging effects on creep rate and reliability in lead free solder joints," *SMTA J.*, vol. 25, no. 3, pp. 19–28, 2012.

[36] X. Zha, "Numerical Analysis of Lead-free Solder Joints : Effects of Thermal Cycling and Electromigration," no. March, 2016.

[37] M. Hasnine, M. Mustafa, J. C. Suhling, B. C. Prorok, M. J. Bozack, and P. Lall, "Characterization of aging effects in lead free solder joints using nanoindentation," in *Proceedings - Electronic Components and Technology Conference*, 2013.

[38] M. Mustafa, Z. Cai, J. C. Roberts, J. C. Suhling, and P. Lall, "Evolution of the tension/compression and shear cyclic stress-strain behavior of lead-free solder subjected to isothermal aging,"

Intersoc. Conf. Therm. Thermomechanical Phenom. Electron. Syst. ITHERM, pp. 765–780, 2012.

[39] R. Al Athamneh *et al.*, "Effect of aging on the fatigue life and shear strength of SAC305 solder joints in actual setting conditions," in *InterSociety Conference on Thermal and Thermomechanical Phenomena in Electronic Systems, ITHERM*, 2019.

[40] A. Lajimi, J. Cugnoni, and J. Botsis, "Reliability Analysis of Lead-free Solders," *Analysis*, 2008.

[41] L. J. Ladani and A. Dasgupta, "Partitioned cyclic fatigue damage evolution model for PB-free solder materials," in *2007 Proceedings of the ASME Pressure Vessels and Piping Conference - 8th International Conference on Creep and Fatigue at Elevated Temperatures - CREEP8*, 2008.

[42] S. Hamasha, L. Wentlent, and P. Borgesen, "Statistical Variations of Solder Joint Fatigue Life Under Realistic Service Conditions," *IEEE Trans. Components, Packag. Manuf. Technol.*, 2015.

[43] S. Su, F. J. J. Akkara, R. Thaper, A. Alkhazali, M. Hamasha, and S. Hamasha, "A state-of-the-art review of fatigue life prediction models for solder joint," *J. Electron. Packag. Trans. ASME*, vol. 141, no. 4, 2019.

[44] R. Darveaux, "Effect of simulation methodology on solder joint crack growth correlation," *Proc. - Electron. Components Technol. Conf.*, 2000.

[45] R. Darveaux, "Effect of simulation methodology on solder joint crack growth correlation and fatigue life prediction," *J. Electron. Packag. Trans. ASME*, 2002.

[46] A. Syed, "Accumulated creep strain and energy density based thermal fatigue life prediction models for SnAgCu solder joints," *2004 Proceedings. 54th Electron. Components Technol. Conf. (IEEE Cat. No.04CH37546)*, no. February, pp. 737–746, 2016.

[47] P. Chauhan, M. Osterman, S. W. R. Lee, and M. Pecht, "Critical review of the engelmaier model for solder joint creep fatigue reliability," *IEEE Transactions on Components and Packaging Technologies*. 2009.

[48] W. Engelmaier and A. I. Attarwala, "Surface-Mount Attachment Reliability of Clip-Leaded Ceramic Chip Carriers on FR-4 Circuit Boards," *IEEE Trans. Components, Hybrids, Manuf. Technol.*, 1989.

[49] W. Engelmaier, "Solder joints in electronics: Design for Reliability," in *TMS Annual Meeting*, 1997.

[50] W. Engelmaier and L. J. Turbini, "Design for reliability in advanced electronic packaging," *SMI Surf. Mt. Int. Adv. Electron. Manufactuting Technol. Proc. Tech. ProgramSMI Surf. Mt. Int. Adv. Electron. Manufactuting Technol. Proc. Tech. Progr.*, 1995.

[51] W. Engelmaier, "Reliability Test.," *Circuits Manuf.*, 1988.

[52] J. P. M. Clech, R. J. Coyle, and B. Arfaei, "Pb-Free Solder Joint Thermo-Mechanical Modeling: State of the Art and Challenges," *JOM*, 2019.

[53] N. Paydar, Y. Tong, H. Akay, and W. Boehmer, "Finite Element Mesh Generation and Analysis of Solder Joints for Fatigue Life Predictions," *Mech. Eng.*, p. 179, 1993.

[54] L. F. Coffin, "A study of the effects of cyclic thermal stresses on a ductile metal," *Transactions of the American Society of Mechanical Engineers*. 1954.

[55] X. Q. Shi, H. L. J. Pang, W. Zhou, and Z. P. Wang, "Modified energy-based low cycle fatigue model for eutectic solder alloy," *Scr. Mater.*, vol. 41, no. 3, pp. 289–296, 1999.

[56] H. D. Solomon, "Fatigue of 60 / 40 Solder," vol. C, no. 4, pp. 423–432, 1987.

[57] H. D. Solomon, "The influence of hold time and fatigue cycle wave shape on the-low cycle fatigue of 60:40 solder.pdf," in *38th Electronics Components Conference 1988., Proceedings*, 1988, pp. 7–12.

[58] Z. Qian and S. Liu, "On the life prediction and accelerated testing of solder joints," in *American Society of Mechanical Engineers, EEP*, 1998.

[59] L. Anand, "Constitutive equations for hot-working of metals," *Int. J. Plast.*, 1985.

[60] S. B. Brown, K. H. Kim, and L. Anand, "An internal variable constitutive model for hot working of metals," *Int. J. Plast.*, 1989.

[61] X. Chen, G. Chen, and M. Sakane, "Modified anand constitutive model for lead-free solder SN-3.5AG," in *Thermomechanical Phenomena in Electronic Systems -Proceedings of the Intersociety Conference*, 2004.

[62] J. Depiver, S. Mallik, and D. Harmanto, "Creep Damage of BGA Solder Interconnects Subjected to Thermal Cycling and Isothermal Ageing," *Electron. Packag. Technol. Conf. IEEE*, no. December, 2019.

[63] J. A. Depiver, S. Mallik, and E. H. Amalu, "Creep Response of Various Solders used in Soldering Ball Grid Array (BGA) on Printed," *IAENG*, vol. 0958, 2019.

[64] Topline, "BGA," 2020. [Online]. Available: https://www.topline.tv/SMD_vrs_NSMD.html. [Accessed: 20-Feb-2019].

[65] B. A. Zahn, "Impact of ball via configurations on solder joint reliability in tape-based, chip-scale packages," in *Proceedings - Electronic Components and Technology Conference*, 2002.

[66] T. T. Nguyen, D. Lee, J. B. Kwak, and S. Park, "Effect of glue on reliability of flip chip BGA packages under thermal cycling," in *Microelectronics Reliability*, 2010.

[67] E. H. Amalu and N. N. Ekere, "Modelling evaluation of Garofalo-Arrhenius creep relation for lead-free solder joints in surface mount electronic component assemblies," *J. Manuf. Syst.*, vol. 39, 2016.

[68] X. Long *et al.*, "Constitutive behaviour and life evaluation of solder joint under the multi-field loadings," *AIP Adv.*, 2018.

[69] H. Beyer, V. Sivasubramaniam, M. Bayer, and S. Hartmann, "Reliability of Lead-free Large Area Solder Joints in IGBT Modules with Respect to Passive and Active Thermal Cycling," in *CIPS 2016 - 9th International Conference on Integrated Power Electronics Systems*, 2019.

[70] S. Stoyanov, C. Bailey, and M. Desmulliez, "Optimisation modelling for thermal fatigue reliability of lead-free interconnects in fine-pitch flip-chip packaging," *Solder. Surf. Mt. Technol.*, 2009.

[71] J. Eckermann *et al.*, "Computational modeling of creep-based fatigue as a means of selecting lead-free solder alloys," *Microelectron. Reliab.*, 2014.

[72] X. Chen, G. Chen, and M. Sakane, "Prediction of stress-strain relationship with an improved anand constitutive model for lead-free solder Sn-3.5Ag," *IEEE Trans. Components Packag. Technol.*, vol. 28, no. 1, pp. 111–116, 2005.

[73] J. Chang, L. Wang, J. Dirk, and X. Xie, "Finite element modeling predicts the effects of voids on thermal shock reliability and thermal resistance of power device," *Weld. J. (Miami, Fla)*, 2006.

[74] Q. Wang *et al.*, "Experimental determination and modification of anand model constants for Pb-free material 95-5Sn4.0Ag0.5Cu," in *EuroSime 2007: International Conference on Thermal, Mechanical and Multi-Physics Simulation Experiments in Microelectronics and Micro-Systems, 2007*, 2007.

[75] L. Zhang *et al.*, "Determination of Anand parameters for SnAgCuCe solder," *Model. Simul. Mater. Sci. Eng.*, 2009.

[76] Trina Barua, "A Comparative Study of The Thermo-Mechanical Behavior of WCSP Assembly Due to Difference In PCBs' Layer Thickness," vol. 8, no. 3, pp. 1–59, 2016.

[77] JEDEC-JESD22-A104D, "Temperature Cycling," 2014.

[78] JEDEC Standard, "Power and Temperature Cycling JESD22-A105C," *JEDEC SOLID STATE Technol. Assoc.*, 2004.

[79] JEDEC Solid State Technology Association and JEDEC, "JEDEC Standard JESD22-A104D, Temperature Cycling," *Jedec.Org*, 2009.

[80] S. S. Manson, "Behavior Of Materials Under Conditions Of Thermal Stress," 1953.

[81] S. Wiese and S. Rzepka, "Time-independent elastic-plastic behaviour of solder materials," in *Microelectronics Reliability*, 2004.

[82] D. R. Shirley, H. R. Ghorbani, and J. K. Spelt, "Effect of primary creep and plasticity in the modeling of thermal fatigue of SnPb and SnAgCu solder joints," *Microelectron. Reliab.*, 2008.

[83] A. R. Syed, "Creep crack growth prediction of solder joints during temperature cycling- an engineering approach," *J. Electron. Packag. Trans. ASME*, 1995.

[84] B. Wong, D. E. Helling, and R. W. Clark, "A Creep-Rupture Model for Two-Phase Eutectic Solders," *IEEE Trans. Components, Hybrids, Manuf. Technol.*, 1988.

[85] A. Syed, "Accumulated creep strain and energy density based thermal fatigue life prediction models for SnAgCu solder joints," in *Proceedings - Electronic Components and Technology Conference*, 2004.

[86] M. M. Hasnine *et al.*, "the Mechanical Behavior of Ceramic," *2007 Proc. 57th Electron. Components Technol. Conf.*, vol. 37, no. 7, pp. 49–53, 2014.

[87] R. Darveaux, K. Banerji, A. Mawer, G. Dody, and J. Lau, "Reliability of plastic ball grid array assembly. In Ball grid array

technology (Vol. 13, pp. 379-442). McGraw-Hill.," *Ball grid array Technol. McGraw-Hill*, vol. 13, pp. 379–442, 1995.

[88] J. Morrow, "Cyclic Plastic Strain Energy and Fatigue of Metals," in *Internal Friction, Damping, and Cyclic Plasticity*, 2009.

[89] F. Ellyin and D. Kujawski, "Plastic strain energy in fatigue failure," *J. Press. Vessel Technol. Trans. ASME*, 1984.

[90] T. An, C. Fang, F. Qin, H. Li, T. Tang, and P. Chen, "Failure study of Sn37Pb PBGA solder joints using temperature cycling, random vibration and combined temperature cycling and random vibration tests," *Microelectron. Reliab.*, 2018.

[91] M. C. Hsieh and S. L. Tzeng, "Solder joint fatigue life prediction in large size and low cost wafer-level chip scale packages," in *Proceedings of the Electronic Packaging Technology Conference, EPTC*, 2014.

[92] J. Mi, Y. F. Li, Y. J. Yang, W. Peng, and H. Z. Huang, "Thermal cycling life prediction of Sn-3.0Ag-0.5Cu solder joint using type-i censored data," *Sci. World J.*, 2014.

[93] E. George, D. Das, M. Osterman, and M. Pecht, "Thermal cycling reliability of lead-free solders (SAC305 and Sn3.5Ag) for high-temperature applications," *IEEE Trans. Device Mater. Reliab.*, 2011.

[94] W. Xie, T. K. Lee, K. C. Liu, and J. Xue, "Pb-Free solder joint reliability of fine pitch chip-scale packages," in *Proceedings - Electronic Components and Technology Conference*, 2010.

[95] F. X. Che, J. H. L. Pang, and L. H. Xu, "IMC consideration in FEA simulation for PB-free solder joint reliability," in *Thermomechanical Phenomena in Electronic Systems - Proceedings of the Intersociety Conference*, 2006.

[96] P. Arulvanan, Z. Zhong, and X. Shi, "Effects of process conditions on reliability, microstructure evolution and failure modes of SnAgCu solder joints," *Microelectron. Reliab.*, 2006.

[97] P. Lall, V. Yadav, J. Suhling, and D. Locker, "A study on the evolution of the high strain rate mechanical properties of SAC105 lead free alloy at high operating temperatures," in *ASME 2015 International Technical Conference and Exhibition on Packaging and Integration of Electronic and Photonic Microsystems, InterPACK 2015, collocated with the ASME 2015 13th International Conference on Nanochannels, Microchannels, and Minichannels*, 2015.

[98] S. W. R. Lee and D. Lau, "Computational model validation with experimental data from temperature cycling tests of PBGA assemblies for the analysis of board level solder joint reliability," in *Proceedings of the 5th International Conference on Thermal and Mechanical Simulation and Experiments in Microelectronics and Microsystems, EuroSimE 2004*, 2004.

[99] L. Zhang, R. Sitaraman, V. Patwardhan, L. Nguyen, and N. Kelkar, "Solder joint reliability model with modified Darveaux's equations for the micro SMD wafer level-chip scale package family," in *Proceedings - Electronic Components and Technology Conference*, 2003.